Raman spectroscopy of gaseous inclusions in EDML ice core: first results – microbubbles

Christian WEIKUSAT, Johannes FREITAG, Sepp KIPFSTUHL

Alfred Wegener Institute for Polar and Marine Research (AWI), Bremerhaven, Germany
E-mail: christian.weikusat@awi.de

ABSTRACT. Measurements of N_2/O_2 ratios inside individual air bubbles at various depths in the EDML (Antarctic) ice core are presented here. The small bubbles (diameter less than ~200 μm) in deeper ice are significantly enriched in O_2 compared to the larger bubbles. The N_2/O_2 ratios show a systematic dependence on bubble size which is not the case for bubbles in shallower ice. This is interpreted as an effect of pressure relaxation during storage of the cores.

INTRODUCTION

Gaseous inclusions in ice cores offer the unique possibility of directly extracting and analysing the atmosphere of the past. Correct interpretation of the results requires a thorough understanding of the processes influencing the air content of the inclusions.

High-resolution gas measurements inside ice cores are of great importance for the accurate reconstruction of palaeoclimatic conditions, which in turn enable more accurate predictions of climate changes. Of special interest are the greenhouse gases (e.g. CH_4, CO_2), but the more easily measurable N_2/O_2 ratios may serve as a proxy for their behaviour and distribution (Bender, 2002; Lüthi and others, 2010). The dynamics of air inclusions in ice and especially the transition from bubbles to crystalline air hydrates (clathrates) pose a challenge to the interpretation of gas measurements, as recent investigations have shown (Lüthi and others, 2010; Schaefer and others, 2011). More detailed data on the general processes affecting mixing ratios in gaseous inclusions are therefore urgently needed.

Two generations of air bubbles can be distinguished in ice sheets. The primary bubbles were formed during accumulation and solidification of snow to ice (including also the microbubbles described by Lipenkov (2000)). With increasing pressure in the ice these bubbles shrink and the contained gases dissolve in the ice. This process can lead to the complete disappearance of smaller bubbles, which has also been shown in laboratory experiments (e.g. Jones and Johari, 1977). Secondary bubbles are formed after the extraction of the ice core and the related decompression. They are filled with gas which had been dissolved in the ice matrix. Microscopic images of ice samples taken on fresh ice just after extraction of the core and several years later from the same samples illustrate this process (Fig. 1). While the clathrates remain stable, several of the initially visible microinclusions (the so-called *black dots* (BD)) developed into bubbles or plate-like inclusions (PLI). The PLI have long been of interest to glaciologists, and their formation has been linked to deformation (Muguruma and others, 1966; Mae, 1968) and also relaxation events (Gow, 1971; Ram and others, 2000). More recent investigations show that PLI contain gas, mainly O_2, which has been interpreted as the effect of the fast diffusion of O_2 through the ice matrix (Nedelcu and others, 2009). The effect of pressure and relaxation on bubbles has also been investigated. Jones and Johari (1977) observed the shrinking and final disappearance of bubbles under pressure, within and outside the clathrate stability field, i.e. the effect is independent of clathrate formation. After the release of pressure, the bubble reappeared. Shoji and Langway (1983, 1985) showed that relaxation and consecutive growth of bubbles occurs mere hours after pressure release. This might also explain the observations of Lipenkov (2000) who observed microbubbles in fresh ice down to the bubble–clathrate transition zone.

Raman spectroscopy has been used before to characterize gases and also to measure liquid and solid inclusions, mainly in petrology (Burke, 2001, and references therein) but also in ice (Pauer and others, 1995; Ikeda and others, 1999; Ikeda-Fukazawa and others, 2001; Bendel, 2009). With the introduction of better instruments and spectrometers, non-destructive in situ measurements of gas-mixing ratios inside individual gaseous inclusions have become possible. To better understand the complex interactions of bubbles and clathrates and the processes of enclathration, we must first understand the general behaviour of gas in ice. This work aims to provide a further step towards advanced understanding of the diffusion process.

METHODS

Samples and preparation

The samples were taken from two ice cores drilled at Kohnen station, Dronning Maud Land, East Antarctica (75°00′ S, 0°04′ E; 2882 m a.s.l.), within the framework of the European Project for Ice Coring in Antarctica (Oerter and others, 2004). The EDML core was drilled in six consecutive seasons from 2001 to 2006 and reached 2774 m depth. The shallow core B34 was drilled in 2004 and reached 200 m depth. For details of the drilling method see Wilhelms and others (2007). The cores have since been stored at –30°C at AWI, Bremerhaven.

The protocols for sample preparation were very similar to those described by Kipfstuhl and others (2006). The samples were cut with a bandsaw. Top and bottom surfaces were microtomed and afterwards smoothed by sublimation. Clear surfaces are essential for the visual detection of the bubbles as well as for the Raman measurements. The samples were then frozen to standard glass slides. In contrast to the method of Kipfstuhl and co-workers we did not use silicon oil, as it produces a very intense Raman spectrum which may mask the comparably weak bands of the gases, especially when measuring small bubbles (Fig. 2). The sample sizes were approximately $30 \times 20 \times 10\,mm^3$.

https://doi.org/10.3189/2012JoG11J222 Published online by Cambridge University Press

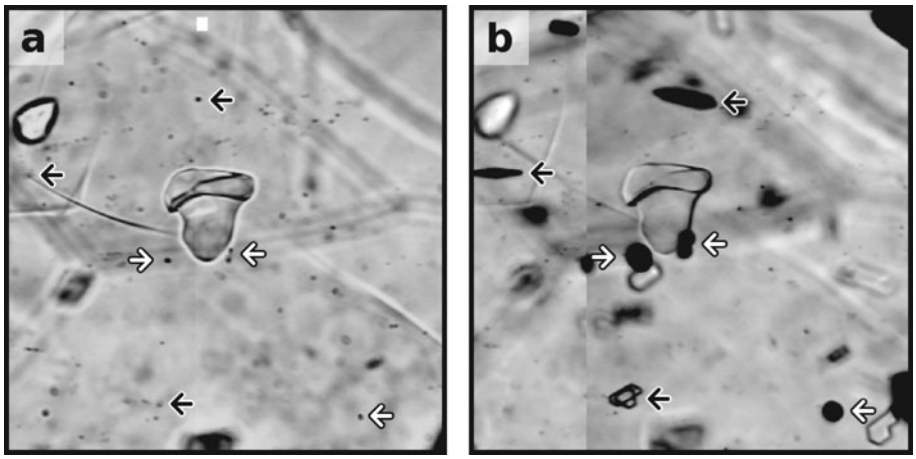

Fig. 1. EDML, 1095 m depth. (a) Freshly drilled core. Various black dots, a large hydrate in the center and a smaller hydrate in the upper left corner. (b) Same sample after 3 years of relaxation. At the locations of some of the black dots, microbubbles (white arrows) or plate-like inclusions (black arrows) have formed. Other black dots appear not to be influenced by relaxation.

Raman spectroscopy

Background

The Raman effect describes the inelastic scattering of light on molecules or molecular groups. When light interacts with the electron clouds of the target, most of it is scattered elastically without any change in energy (*Rayleigh scattering*). About one in every 10^8 photons is scattered inelastically, i.e. energy is transferred either from the photon to a vibrational motion of the nuclei (*Stokes scattering*) or an already active vibration transfers its energy to the photon (*anti-Stokes scattering*). In the Raman spectrometer the elastically scattered light is filtered out and the frequency-shifted parts are passed to the detector. The resulting spectrum shows the Raman shift relative to the incident laser wavelength, where the values on the abscissa (conventionally given in relative wavenumbers) directly betray the energies of the involved vibrations. These energies are influenced by environmental conditions (e.g. pressure), neighbouring atoms (chemistry) and, in the case of crystalline materials, the short-range order of the crystal structure. The resulting Raman spectrum is unique to the phase of the target and is thus widely used in chemistry, geosciences and other fields as a fingerprinting technique for the identification of phases in gaseous, liquid and solid materials. It is important to have good-quality spectra where many bands can be detected. The identification of phases based on the position of only a single Raman band must remain speculative and should be avoided. After careful calibration, the Raman shift can also be used for pressure measurements (e.g. Gu and others, 2000).

To extract the band parameters (peak position, width, height) from the spectrum, suitable functions (usually Voigt or Gauss–Lorentz) are mathematically fitted to the Raman bands. Many commercial as well as free software packages are available for this purpose (e.g. Wojdyr, 2010). For a reliable interpretation of band parameters, additional data treatment (e.g. smoothing algorithms) must be avoided as they can alter the band parameters and the relative intensities of the bands. It is therefore essential to acquire high-quality spectra from the start. The signal-to-noise ratio can be improved by prolonging the acquisition time and/or acquiring and combining a larger number of spectra for each point. In this paper, all spectra are presented as acquired.

For a more detailed view of this method and the selection rules that make a vibration Raman-active see any of the available textbooks (e.g. Smith and Dent, 2005).

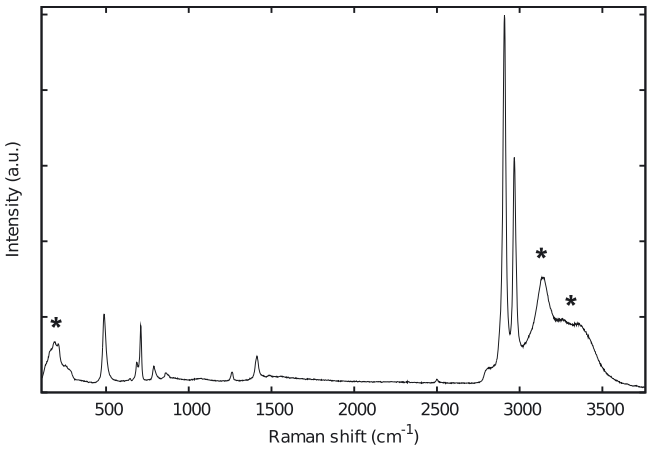

Fig. 2. Raman spectrum of an ice sample coated with silicon oil. Raman bands marked with an asterisk belong to the ice matrix (see Fig. 3).

Instrument

We used a WITec alpha300 R spectrometer with a frequency-doubled NdYAG laser ($\lambda = 532$ nm), a grating with 600 grooves mm^{-1}, a Peltier-cooled Electron Multiplying Charge Coupled Device (EMCCD) detector and a long working distance 50× microscope objective with numerical aperture of 0.35. The instrument was calibrated using the Raman spectrum of a monocrystalline silicon wafer. Acquisition times used varied between 1 and 120 s per spectrum, with five to ten spectra combined for each spot, depending on the signal intensity.

During measurement, the samples were held at –15°C in a specially adapted cooling cell mounted directly to the motorized XY-stage of the spectrometer. The cell was cooled with a LAUDA RC6CP compact low-temperature thermostat and purged with dry cold nitrogen gas to prevent the formation of frost. The purging gas pressure must be chosen carefully so that the sample does not suffer enhanced sublimation. Gas pressures of ∼2 bar were found to be

https://doi.org/10.3189/2012JoG11J222 Published online by Cambridge University Press

sufficient to prevent frost while not being too detrimental to the sample surface. To ascertain the feasibility of purging with nitrogen gas while measuring N_2/O_2 ratios, abundant measurements of the ice matrix were performed at various depths inside the samples. None of these measurements showed any traces of the N_2 Raman bands (Fig. 3, middle), so we conclude that the purging gas does not influence the measurements. This result enables the use of nitrogen gas for purging which is much cheaper and also more readily available than, for instance, argon or helium.

Peak fitting and calibration

After subtraction of a polynomial background, Voigt functions were fitted to the Raman bands with the open-source software package FITYK 1.0.1 (Wojdyr, 2010). Peak intensities of the main vibrational bands (N_2 ~2335 cm^{-1}, O_2 ~1560 cm^{-1}) were used to calculate the N_2/O_2 ratios. While the integrated peak areas can also be used and do show the same trends, they were found to have a much larger scatter than the peak intensities. To enable quantification of the mixing ratios, a calibration factor for the instrument response had to be obtained. We therefore conducted several measurements of room air (Fig. 3, top) on different days and with varying acquisition times. All air measurements were made before setting up the cooling cell, so that the possibility of biases from liquid or gaseous nitrogen used for cooling purposes can be disregarded. The results show good reproducibility and yield a raw ratio of 3.03 ± 0.07 (mean value and standard deviation of all air measurements). Assuming the laboratory air has standard atmospheric composition (i.e. N_2/O_2=3.73) we adopted a correction factor of 1.23 for the subsequent measurements.

Image analysis

Every measured bubble was photographed with the built-in camera of the Raman spectrometer. The bubble diameters were obtained from these photos with the free image analysis software ImageJ (Abràmoff and others, 2004). In case of aspherical bubbles, the longest possible diameter was used. While the values thus obtained also provide a good estimate of volume for the smaller, well-rounded bubbles, they are certainly less meaningful for the larger and more irregularly shaped objects.

Computer tomography

A representative sample from the transition zone (EDML 914 m) was analysed by computer tomography to obtain information about bubble sizes, shapes and distribution. The instrument used is a full-core tomograph with a Fraunhofer IIS XEye 4000×2000 pixel detector, where 1 pixel $\widehat{=}$ 100 μm (binning 2×). The focal spot size is 20 μm.

A Feinfocus 225 kV tube was used as the X-ray source. The measurement settings applied were 140 kV tube voltage and 380 μA tube current. The method was Helix CT with vertical feed of the ice core during rotation and 3200 measurement steps per degree. The achieved resolution was 28.15 μm per voxel. The sample used was half the ice core, resulting in a maximum irradiated length of ~10 cm. The size and shape of the detected bubbles (n = 14 684) were evaluated. The employed shapefactor f is defined as

$$f = 6\sqrt{\pi}\frac{V}{\sqrt{S^3}}$$

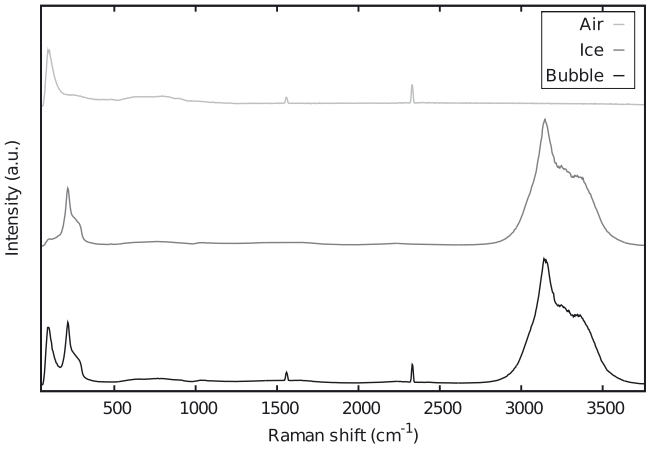

Fig. 3. Raman spectra of (top) room air, (middle) ice matrix and (bottom) bubble in the ice.

where V is the volume and S the surface area of the bubble. For a perfect sphere f = 1, and f = 0.90 for a prolate spheroid with (major axis)/(minor axis) = 2. We define *spheric bubbles* as those with a shapefactor f between 0.95 and 1.

RESULTS

Raman spectroscopy

Figure 3 shows the Raman spectra of room air, pure ice and a bubble inside the ice. The main Raman bands of the N_2 and O_2 vibrations are indicated for air and bubble. The peak at ~100 cm^{-1} has not been described in the literature before. From our current work and also measurements of other gases it is evident that it is caused by some vibrations of N_2 and O_2. As this peak is very intense it can be used for fast tracking of gaseous inclusions in larger ice volumes. The spectrum of the bubble in ice is a combination of the ice spectrum with the Raman bands of the gases contained in the bubble. The measured bubbles are very small and the measurements were done through several millimeters of ice, so even with a good confocal set-up, the spectra of the bubble will always show bands from lattice and OH vibrations of the ice matrix. Figure 4a shows the N_2/O_2 ratios of individual bubbles as a function of diameter for a wide selection of depths (454–1023 m), including depths lying inside the bubble–clathrate transition zone. The overall trends are similar at all shown depths.

The larger bubbles (diameter >200 μm) show a rather size-independent distribution of gas-mixing ratios. For the depths above the bubble–clathrate transition, all values scatter around the recent atmospheric ratio of 3.7. The larger bubbles inside the transition zone have distinctly higher ratios than bubbles at other depths, i.e. they are oxygen-depleted, as has been shown by Ikeda and others (1999). Mixing ratios of the smaller bubbles (diameter <200 μm) change as a function of the diameter, with the smallest bubbles exhibiting the lowest N_2/O_2 ratios (the highest relative O_2 contents). In the bubble–clathrate transition zone, no bubbles were found in the diameter range from ~120 to ~200 μm, resulting in a more-or-less bimodal distribution for the overall bubble sizes. It is important to note that all small bubbles (occasional outliers excepted) have ratios well below 3, with the vast majority of ratios lying in the range below 2. A considerable number of the smaller bubbles

https://doi.org/10.3189/2012JoG11J222 Published online by Cambridge University Press

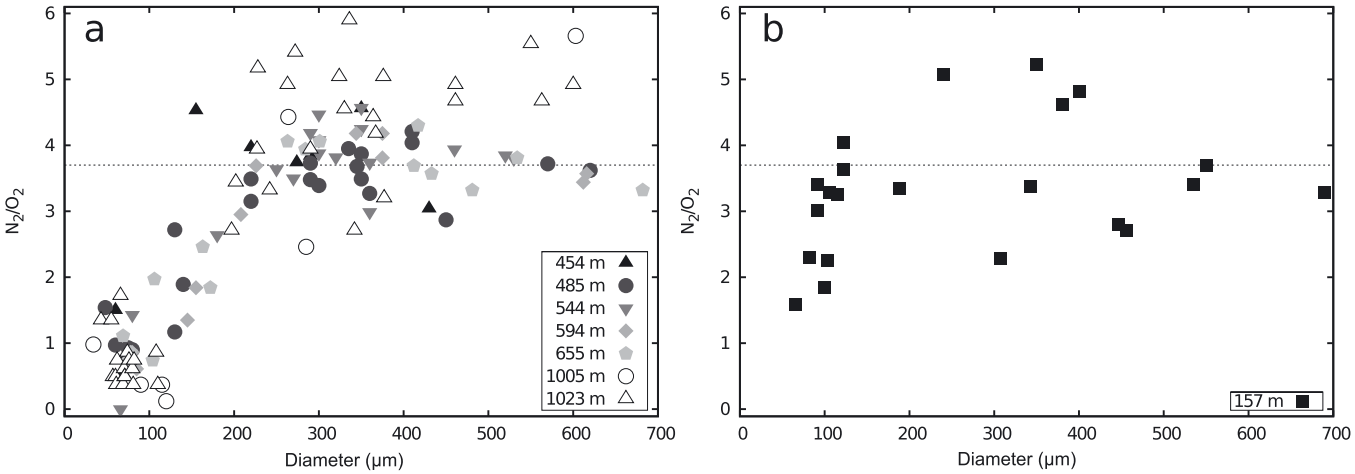

Fig. 4. N_2/O_2 ratios as a function of bubble diameter for several depths. Solid symbols show depths where only bubbles occur, while open symbols mark depths inside the bubble–clathrate transition zone. The dashed line represents the recent atmospheric value of 3.73. (a) Bubbles with diameters less than 200 μm are enriched in O_2, with N_2/O_2 ratios down to 0 (only O_2) and the majority less than 2. (b) In shallow ice no small bubbles fall below 1.6 and the majority have ratios above 3. The scatter is larger than for deeper ice.

display ratios below 1, meaning that these bubbles contain more oxygen than nitrogen. Some bubbles even show ratios at or very close to zero, i.e. they only contain oxygen and no nitrogen.

For reference purposes we also analysed a depth close to the firn–ice transition (B34 157 m). The ice at this depth has not encountered high pressures in situ, and therefore should not show effects produced by extended relaxation and related changes in structure and microstructure. The results of the measurements are shown in Figure 4b, which is shown on the same scale as Figure 4a. The larger bubbles also appear to be scattered around the atmospheric value, although the deviation from this value is much larger than at the other depths. For the smaller bubbles, the measured ratios differ distinctly from the results shown in Figure 4a. Most of the smaller bubbles at B34 157 m exhibit ratios well above 3, with maximum values exceeding 4. Even for the smallest bubbles, none of the measured ratios falls below 1.5, so no bubble at this depth contains more oxygen than nitrogen. Furthermore, a functional dependency of the mixing ratios on bubble sizes cannot be seen at this depth.

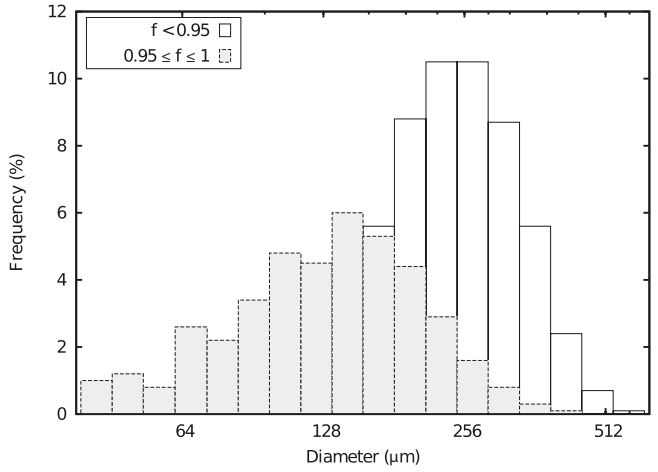

Fig. 5. Percentage of size distribution of spherical ($f > 0.95$) and aspherical bubbles ($f < 0.95$) in EDML (914 m) as a function of diameter (shown as equivalent diameter of a sphere of same volume). The absolute number of bubbles is $n = 14\,684$. For a detailed explanation of f see text.

Computer tomography

Computer tomographic analysis of a very large number of bubbles ($n = 14\,684$) inside the transition zone clearly shows that the smaller bubbles are distinctly more round than the larger bubbles (Fig. 5). This is in agreement with the results presented by Lipenkov (2000). The diameter for the maximum of the spherical bubbles is around 150–200 μm whereas the maximum for the aspherical and elongated bubbles is around 250–300 μm.

DISCUSSION

The N_2/O_2 mixing ratios in air bubbles from deep ice cores differ systematically in bubbles of different sizes. The large bubbles (diameters above ~200 μm) have ratios that scatter around the atmospheric value, with absolute values varying with depth. Small bubbles (diameters less than ~200 μm) have very low N_2/O_2 ratios, i.e. they are enriched in oxygen. Furthermore, the small bubbles show a size-dependent distribution of mixing ratios, with the lowest values (highest oxygen contents) in the smallest bubbles. In shallower ice, just below the bubble close-off (firn–ice transition), all bubbles scatter approximately around the atmospheric value, without obvious functional dependence on the bubble size. The variability of ratios betweeen different bubbles and microbubbles is rather larger than in deeper ice (Fig. 4b). All bubbles measured at this depth are from the same layer (cm thick), so climatic effects can be ruled out as the cause. N_2/O_2 variabilities in shallow depths have been described as fractionation effects before or during pore close-off (e.g. Enting, 1985; Huber and others, 2006; Severinghaus and Battle, 2006; Fujita and others, 2009). However, the variations we have measured even between neighbouring bubbles are larger by far than the fractionation-dependent variations proposed in the literature. The small bubbles less than ~200 μm in diameter behave very differently from bubbles in deeper ice. Most of them show N_2/O_2 ratios

https://doi.org/10.3189/2012JoG11J222 Published online by Cambridge University Press

greater than 3, while none of them have ratios less than 1.5, both of which have not been found in deeper ice.

After the bubbles have formed they are submitted to gradually rising hydrostatic pressures in the thickening ice sheet. When the pressure in the bubbles exceeds the equilibrium pressure, gas molecules are dissolved as solid solutions in the ice matrix and small bubbles will eventually vanish completely. Given the higher curvature of the small bubbles, a higher pressure and a diffusion from small to large bubbles should be expected. Due to the higher diffusion constant and flux of O_2 compared to N_2 (Ikeda-Fukazawa and others, 2005; Hondoh, 2009), this would result in the small bubbles being depleted of oxygen, i.e. their N_2/O_2 ratios would be higher than for larger bubbles. This cannot be seen in our data, so other processes must be considered. When the pressure is released at excavation of the core, the gases dissolved in the ice matrix become supersaturated and start to form gaseous micro-inclusions. The type of the newly forming inclusion is dependent on the local microstructure of the ice matrix: bubbles grow at the location of solid micro-inclusions, whereas areas of accumulated crystal defects may evolve into plate-like inclusions. Due to the differences in diffusion rates, growing secondary inclusions are initially filled with oxygen and will therefore always exhibit much lower N_2/O_2 ratios than other bubbles. This is in excellent agreement with our data. The shrinking and vanishing of small bubbles with pressure and their reappearance after pressure release have been observed experimentally by Jones and Johari (1977), and our results confirm their conclusions. Further evidence for a secondary growth of the small bubbles can be found by evaluating their shape. Younger bubbles should be more rounded than older bubbles, as they have not been influenced by deformation and flow of the ice. Our computer tomographic measurements show a clear correlation of the bubble size with shape, with the spherical bubbles being significantly smaller than the aspherical bubbles. The maximum of the spherical bubbles is $\sim$200 μm, which is in good agreement with the results from Raman spectroscopy.

As microbubbles in all regimes (i.e. with and without directly neighbouring bubbles and/or clathrates) show similar behaviour, it is likely that the gas comes directly from the ice matrix and not via diffusion from other gaseous inclusions.

The higher N_2/O_2 ratios in bubbles from the transition zone agree well with the predictions of Salamatin and others (1999) and the data of Ikeda and others (1999). The relative enrichment in O_2 is believed to stem from the faster diffusion of oxygen to the newly forming clathrates (Ikeda-Fukazawa and others, 2001).

Why microbubbles start to grow only on some of the initially visible micro-inclusions will be a topic of further research. It may be related to the varying chemistry of solid micro-inclusions which has been verified by Raman spectroscopy (e.g. Ohno and others, 2006; Sakurai and others, 2009, 2010, and references therein).

CONCLUSION

The small round bubbles enriched in O_2 constitute a second generation of air bubbles which have grown due to pressure release and relaxation of the ice cores during storage. Our results agree well with the experimental findings by Jones and Johari (1977). A proposed diffusion of gases from small to large bubbles that would result in higher N_2/O_2 ratios in the microbubbles cannot be seen in our data. Yet this process could be masked by the more intense relaxation effects.

Based on the results presented here, more systematic investigations will follow to further clarify the interrelations between pressure relaxation, ice microstructure and the growth of secondary gaseous inclusions. Our ongoing studies will focus on the bubble–clathrate transition zone, clarifying the fractionation effects during the growth of clathrate hydrates. Measurements of different layers in the shallow cores and Raman spectroscopic pressure measurements inside individual bubbles will provide more information on fractionation effects during pore close-off. Conventional gas measurements require larger volumes of ice, so the significant variations between neighbouring bubbles in the shallow core are smoothed out. Enhanced theories about fractionation during pore close-off are needed to explain our data.

ACKNOWLEDGEMENTS

We thank G. Nehrke and E. Dunker for planning and construction of the cooling cell, and two anonymous reviewers for constructive remarks. This work was funded by German Research Foundation (DFG) grant WE4771/1.

REFERENCES

Abràmoff MD, Magalhães PJ and Ram SJ (2004) Image processing with ImageJ. *Biophoton. Int.,* **11**(7), 36–42

Bendel V (2009) Untersuchung an Luftblasen im EDML-Eisbohrkern mit Bildanalyse und Ramanspektroskopie. (Master's thesis, Universität Göttingen)

Bender ML (2002) Orbital tuning chronology for the Vostok climate record supported by trapped gas composition. *Earth Planet. Sci. Lett.,* **204**(1–2), 275–289 (doi: 10.1016/S0012-821X(02)00980-9)

Burke EAJ (2001) Raman microspectrometry of fluid inclusions. *Lithos,* **55**(1–4), 139–158 (doi: 10.1016/S0024-4937(00)00043-8)

Enting IG (1985) A lattice statistics model for the age distribution of air bubbles in polar ice. *Nature,* **315**(6021), 654–655

Fujita S, Okuyama J, Hori A and Hondoh T (2009) Metamorphism of stratified firn at Dome Fuji, Antarctica: a mechanism for local insolation modulation of gas transport conditions during bubble close off. *J. Geophys. Res.,* **114**(F3), F03023 (doi: 10.1029/2008JF001143)

Gow AJ (1971) Relaxation of ice in deep drill cores from Antarctica. *J. Geophys. Res.,* **76**(11), 2533–2541

Gu Y, Zhou Y, Tang H, Rothe EW and Reck GP (2000) Pressure dependence of vibrational Raman scattering of narrow-band, 248-nm, laser light by H_2, N_2, O_2, CO_2, CH_4, C_2H_6, and C_3H_8 as high as 97 bar. *Appl. Phys. B,* **71**(6), 865–871 (doi: 10.1007/s003400000412)

Hondoh T (2009) An overview of microphysical processes in ice sheets: towards nanoglaciology. In Hondoh T ed. *Physics of ice core records II.* Hokkaido University Press, Sapporo, 1–23 (Supplement Issue of Low Temperature Science 68)

Huber C and 7 others (2006) Evidence for molecular size dependent gas fractionation in firn air derived from noble gases, oxygen, and nitrogen measurements. *Earth Planet. Sci. Lett.,* **243**(1–2), 61–73 (doi: 10.1016/j.epsl.2005.12.036)

Ikeda T and 7 others (1999) Extreme fractionation of gases caused by formation of clathrate hydrates in Vostok Antarctic ice. *Geophys. Res. Lett.,* **26**(1), 91–94

Ikeda-Fukazawa T, Hondoh T, Fukumura T, Fukazawa H and Mae S (2001) Variation in N_2/O_2 ratio of occluded air in Dome Fuji

https://doi.org/10.3189/2012JoG11J222 Published online by Cambridge University Press

antarctic ice. *J. Geophys. Res.,* **106**(D16), 17 799–17 810 (doi: 10.1029/2000JD000104)
Ikeda-Fukazawa T and 6 others (2005) Effects of molecular diffusion on trapped gas composition in polar ice cores. *Earth Planet. Sci. Lett.,* **229**(3–4), 183–192 (doi: 10.1016/j.epsl.2004.11.011)
Jones SJ and Johari GP (1977) Effect of hydrostatic pressure on bubbles in ice. *IAHS Publ.* 118 (Symposium at Grenoble 1975 – *Isotopes and Impurities in Snow and Ice*), 23–28
Kipfstuhl S and 6 others (2006) Microstructure mapping: a new method for imaging deformation-induced microstructural features of ice on the grain scale. *J. Glaciol.,* **52**(178), 398–406 (doi: 10.3189/172756506781828647)
Lipenkov VYa (2000) Air bubbles and air-hydrate crystals in the Vostok ice core. In Hondoh T ed. *Physics of ice core records.* Hokkaido University Press, Sapporo, 327–358
Lüthi D and 10 others (2010) CO_2 and O_2/N_2 variations in and just below the bubble–clathrate transformation zone of Antarctic ice cores. *Earth Planet. Sci. Lett.,* **297**(1–2), 226–233 (doi: 10.1016/j.epsl.2010.06.023)
Mae S (1968) Void formation during non-basal glide in ice single crystals under tension. *Philos. Mag.,* **18**(151), 101–114
Muguruma J, Mae S and Higashi A (1966) Void formation by non-basal glide in ice single crystals. *Philos. Mag.,* **13**(123), 625–629 (doi: 10.1080/14786436608212656)
Nedelcu AF, Faria SH and Kuhs WF (2009) Correspondence. Raman spectra of plate-like inclusions in the EPICA-DML (Antarctica) ice core. *J. Glaciol.,* **55**(189), 183–184 (doi: 10.3189/002214309788609010)
Oerter H, Graf W, Meyer H and Wilhelms F (2004) The EPICA ice core from Dronning Maud Land: first results from stable-isotope measurements. *Ann. Glaciol.,* **39**, 307–312 (doi: 10.3189/172756404781814032)
Ohno H, Igarashi M and Hondoh T (2006) Characteristics of salt inclusions in polar ice from Dome Fuji, East Antarctica. *Geophys. Res. Lett.,* **33**(8), L08501 (doi: 10.1029/2006GL025774)
Pauer F, Kipfstuhl J and Kuhs WF (1995) Raman spectroscopic study on the nitrogen/oxygen ratio in natural ice clathrates in the GRIP ice core. *Geophys. Res. Lett.,* **22**(8), 969–971
Ram M, Donarummo J, Jr, Stolz MR and Koenig G (2000) Calibration of laser-light scattering measurements of dust concentration for Wisconsinan GISP2 ice using instrumental neutron activation analysis of aluminum: results and discussion. *J. Geophys. Res.,* **105**(D20), 24 731–24 738 (doi: 10.1029/2000JD900321)
Sakurai T and 6 others (2009) Direct observation of salts as micro-inclusions in the Greenland GRIP ice core. *J. Glaciol.,* **55**(193), 777–783 (doi: 10.3189/002214309790152483)
Sakurai T, Ohno H, Horikawa S, Iizuka Y, Uchida T and Hondoh T (2010) A technique for measuring microparticles in polar ice using micro-Raman spectroscopy. *Int. J. Spectrosc.,* **2010**, 384956 (doi: 10.1155/2010/384956)
Salamatin AN, Lipenkov VY, Hondoh T and Ikeda T (1999) Simulated features of the air-hydrate formation process in the Antarctic ice sheet at Vostok. *Ann. Glaciol.,* **29**, 191–201 (doi: 10.3189/172756499781821571)
Schaefer H, Lourantou A, Chappellaz J, Lüthi D, Bereiter B and Barnola J-M (2011) On the suitability of partially clathrated ice for analysis of concentration and $\delta^{13}C$ of palaeo-atmospheric CO_2. *Earth Planet. Sci. Lett.,* **307**(3–4), 334–340 (doi: 10.1016/j.epsl.2011.05.007)
Severinghaus JP and Battle MO (2006) Fractionation of gases in polar ice during bubble close-off: new constraints from firn air Ne, Kr and Xe observations. *Earth Planet. Sci. Lett.,* **244**(1–2), 474–500 (doi: 10.1016/j.epsl.2006.01.032)
Shoji H and Langway CC, Jr (1983) Volume relaxation of air inclusions in a fresh ice core. *J. Phys. Chem.*, **87**(21), 4111–4114 (doi: 10.1021/j100244a600)
Shoji H and Langway CC, Jr (1985) Mechanical properties of fresh ice core from Dye 3, Greenland. In Langway CC, Oeschger H and Dansgaard W eds. *Greenland ice core: geophysics, geochemistry, and the environment.* American Geophysical Union, Washington, DC, 39–48 (Geophysical Monograph 33)
Smith E and Dent G (2005) *Modern Raman spectroscopy: a practical approach,* Wiley, Chichester
Wilhelms F, Sheldon SG, Hamann I and Kipfstuhl S (2007) Implications for and findings from deep ice core drillings – an example: the ultimate tensile strength of ice at high strain rates. In Kuhs WF ed. *Physics and chemistry of ice.* Royal Society of Chemistry, Cambridge, 635–639 (Special Publication 311)
Wojdyr M (2010) Fityk: a general-purpose peak fitting program. *J. Appl. Crystallogr.,* **43**(5 Pt 1), 1126–1128 (doi: 10.1107/S0021889810030499)

MS received 24 October 2011 and accepted in revised form 2 February 2012